

**Shijin WANG**, Ph.D.<sup>1</sup>

(Corresponding author)

E-mail: shijin\_wang@nuaa.edu.cn

**Rongrong DUAN**, Master's degree candidate<sup>1</sup>

E-mail: duanrongrong@nuaa.edu.cn

**Jiewen CHU**, Master's degree candidate<sup>1</sup>

E-mail: 421707865@qq.com

**Jiahao LI**<sup>2</sup>

E-mail: 920728951@qq.com

**Baotian YANG**, Master's degree candidate<sup>1</sup>

E-mail: 1756495209@qq.com

<sup>1</sup> School of Civil Aviation

Nanjing University of Aeronautics and Astronautics  
No.29, Jiangjun Avenue, Jiangning District, Nanjing,  
210016, China

<sup>2</sup> ZTE Corporation

No.50, Ruanjian Avenue, Yuhuatai District, Nanjing,  
210012, China

Science in Traffic and Transport

Original Scientific Paper

Submitted: 9 June 2022

Accepted: 13 Sep. 2022

# MULTI-FLIGHT REROUTING OPTIMISATION BASED ON TYPICAL FLIGHT PATHS UNDER CONVECTIVE WEATHER IN THE TERMINAL AREA

## ABSTRACT

*With the rapid growth of flight volume, the impact of convective weather on flight operations in the terminal area has become more and more serious. In this paper, the typical flight paths (TFPs) are used to replace flight procedures as the routine flight paths in the terminal area, and the TFP of each flight is predicted by Random Forest (RF), Boosting Tree (BT) and K-Nearest Neighbour (KNN) algorithms based on the weather and flight plan characteristics. A multi-flight rerouting optimisation model by bi-level programming is established, which contains a flight flow optimisation model in the upper layer and a single flight path optimisation model in the lower layer. The simulated annealing algorithm and the bidirectional A\* algorithm are used to solve the upper and lower models. This paper uses the terminal area of Guangzhou Baiyun Airport (ZGGG) and Wuhan Tianhe Airport (ZHHH) for case analysis. The RF algorithm has better performance in predicting TFPs compared with the BT and KNN algorithms. Compared to the historical radar trajectory, the flight path optimisation results show that for the Guangzhou terminal area, while meeting the Terminal Airspace Availability (TAA) as constraint, the flight flow increases and the flight distance reduces, effectively improving the operational efficiency within the terminal.*

## KEYWORDS

*terminal area; convective weather; typical flight path; terminal airspace availability; path optimisation; machine learning.*

## 1. INTRODUCTION

In recent years, with the rapid growth of flight volume, flight delay has become increasingly serious, and convective weather is the most important cause of flight irregularities [1]. According to the operation monitoring centre of the Civil Aviation Administration of China (CAAC), the flight irregularity rate in China due to weather was 51.28%, 47.46%, 46.49%, 57.31% and 59.56% between 2017 and 2021, with an average value of 52.42%, as shown in *Figure 1*. Therefore, flight delay caused by convective weather is a key issue, affecting the sustainable and rapid development of the air transportation industry. Reducing the impact of convective weather on flight operations and reducing flight delay is one of the most important research topics for the civil aviation industry in the future.

Terminal airspace is a narrow airspace connecting en route and airport, in which the departure and arrival of flights are accomplished by changing the altitude, direction and speed [2]. As the terminal airspace is a convergence area of arrival and departure traffic flow, it is characterised by complex route structure, intensive traffic activities, frequent flight conflicts and narrow mobile space. It is a bottleneck for air traffic management, and its ability to cope with weather changes is poor, which easily causes flight delays. With the accumulation

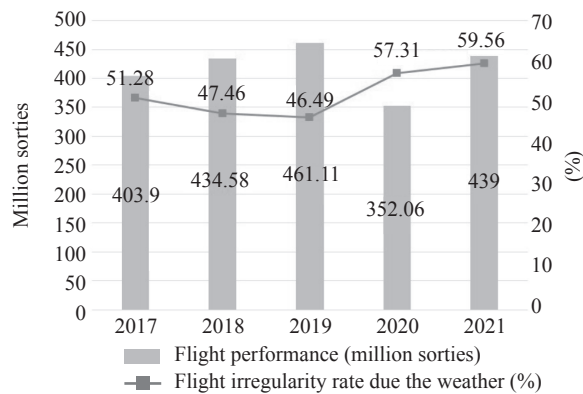


Figure 1 – Number of flights and flight irregularity rate due to weather from 2017 to 2021

and propagation of flight delays, the operational efficiency of the local area and even the whole air traffic system can be reduced to a different extent.

Many scholars are interested in researching the impact of convective weather on flight operations [3–5]. This paper focuses on flight path optimisation in the terminal area under convective weather, aiming to enhance airspace utilisation, reduce flight delays and improve the operational efficiency of the air traffic system. Flight path optimisation refers to finding the optimal flight path with the goal of shorter flight distances or less fuel consumption under the condition of avoiding convective weather, obstacles and other restricted areas. Previous experts and scholars have studied the flight path optimisation problem from multiple perspectives. According to weather changes, the flight path optimisation is divided into static path optimisation and dynamic path optimisation. Sridhar [6] used a playbook and coded departure paths to achieve tactical reroute near congested airspace, and Dwight [7] et al. considered weather forecasts and errors to achieve flight conflict resolution and reroute forecasts. They both implement static path optimisation. Isaacson [8] et al. provided Dynamic Routing for Arrivals in Weather (DRAW) for air traffic controllers to reduce the impact of convective weather on arrival flight operations. Wang [9] et al. predicted the boundary of the severe weather danger zone while achieving flight path optimisation. They both implement dynamic path optimisation. Flight path optimisation can also be classified as single-objective path optimisation [10] and multi-objective path optimisation [11–13] according to the number of objectives of the optimisation model. Single-objective path optimisation selects one of the conditions such as shortest flight distance, shortest flight time and

least fuel consumption as the objective function while multi-objective path optimisation considers multiple conditions comprehensively to form the objective function. Wang [10] et al. designed a three-stage method to study the reroute optimisation with the shortest distance as the objective and the minimum distance of segment, the danger zone and the turning angle as the constraints. Soler [11] et al. conducted 4D trajectory planning with minimised fuel consumption, CO<sub>2</sub> pollution, passenger flight time and sustained trajectory formation as the overall flight cost. Zhang [12] et al. identified scattered hazard areas based on the characteristics of the Bézier curves and Doppler radar, generated smooth and corner curve segments that make up the reroute, and obtained the optimal reroute through multi-objective planning. Taylor [13] et al. used a multi-objective genetic algorithm to generate selectable optimised flight paths for multiple flights based on multiple criteria of operational acceptability.

Flight path solving algorithms are mainly classified into graph-theoretic algorithms, meta-heuristic optimisation algorithms and machine learning algorithms. The graph-theoretic algorithms mainly include algorithms such as the K shortest path algorithm [14] and A\* algorithm [15]. The meta-heuristic optimisation algorithms mainly involve the ant colony optimisation algorithm [16], genetic algorithm [17, 18], simulated annealing algorithm [19, 20] and the SB-RRT\* algorithm (Scenario-Based Rapidly-exploring Random Tree\*) [21]. Machine learning algorithms include the RNN algorithm [22], HMM algorithm [23], CGAN algorithm [24], etc.

So far, although many research results have been achieved on the flight path optimisation problem, the following deficiencies and potentials for improvement still exist: (1) the flight path optimisation failed to draw on historical flight experience and did not consider historical flight paths. (2) The flight path optimisation ignored the specific impact of the severity of convective weather on the capacity of the terminal area and regarded all the airspace affected by convective weather as unflyable airspace. (3) Most of the previous flight path optimisations only consider a single flight, and there are not many research results on the optimisation of multiple flight paths from the system perspective. To overcome the above research shortcomings, this paper uses the RF, BT and KNN

algorithms to predict TFPs and considers the corresponding results as the initial conditions for flight path optimisation as well as calculates the airspace availability in the terminal area under convective weather as the constraints for flight path optimisation. This paper takes into account the interests of terminal area airspace managers and flight operators and constructs a multi-flight rerouting optimisation model with the objectives of maximising terminal area traffic and minimising reroute distance of every single flight to complete flight path optimisation in the terminal area under convective weather conditions.

The structure of this paper is as follows: Section 2 describes the implementation and prediction method of TFPs and the calculation method of the TAA; Section 3 details the process of flight path optimisation in the terminal area, the composition of the multi-flight rerouting optimisation model, and the solution algorithm; Section 4 takes ZGGG and ZHHH terminal area as the research object, determines the prediction algorithm of the TFP and gives case analysis of the flight path optimisation; Section 5 states the summary and research prospect.

## 2. MULTI-FLIGHT REROUTE OPTIMISATION

### 2.1 Obtaining TFPs by OPTICS algorithm

As shown in Figure 2, even under clear weather, quite a few flights deviate from the flight procedure due to airspace environmental constraints and flight habits. To determine the actual flight paths in the terminal area, this paper first clusters the historical flight radar trajectories to obtain

the TFPs in the terminal area under clear weather to reflect the real paths of historical flights. Here, the actual TFP obtained from the historical flight can be used as the initial condition for the path optimisation of the flight to be optimised described in Section 3.3. Therefore, the flight path optimisation process could take into account the flight patterns under historical situations. While giving basic restrictions to the flight path, the optimisation results can be consistent with the objective flight tendency of pilots and the control habits of controllers in the terminal area under convective weather.

#### The process of OPTICS

In this paper, the Ordering Point to Identify the Cluster Structure (OPTICS) algorithm [25] is used to complete the trajectory clustering in two stages-cluster sequence generation and cluster label acquisition. The details are shown in Figure 3.

The process of cluster sequence generation is shown in Figure 4a and the generation result shows that each trajectory only has two values: the core distance (*coreDist*) and reachable distance (*reachDist*). Through the input parameters which are the neighbourhood radius  $\epsilon$  and the minimum number of samples *MinPts* within  $\epsilon$ -radius, the expansion sequence of all samples is generated by calculating *coreDist* and *reachDist* of each sample. The *coreDist* is the minimum neighbourhood radius that makes sample  $x$  a core object, as shown in Equation 1. The *reachDist* is the minimum neighbourhood radius that both makes sample  $x$  a core object and sample  $y$  directly reachable from sample  $x$ , that is, the bigger one of the *coreDist* of sample  $x$  and the distance from sample  $x$  to sample  $y$ , as shown in Equation 2.  $N(x)$  is the number of samples contained

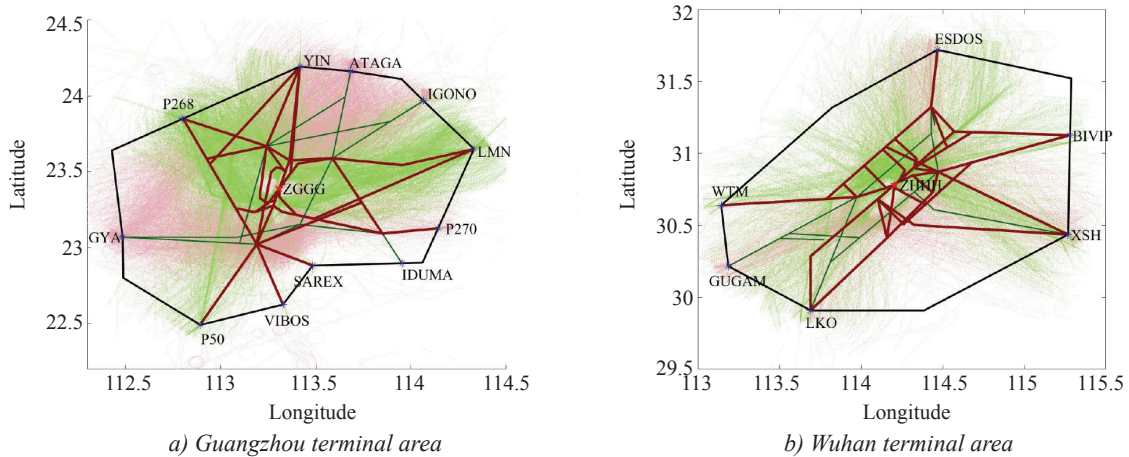


Figure 2 – Radar trajectories and flight procedures in the terminal area

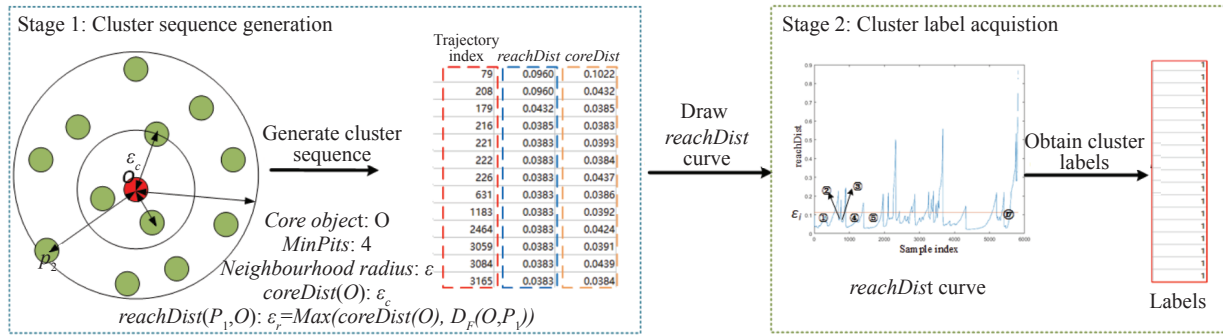
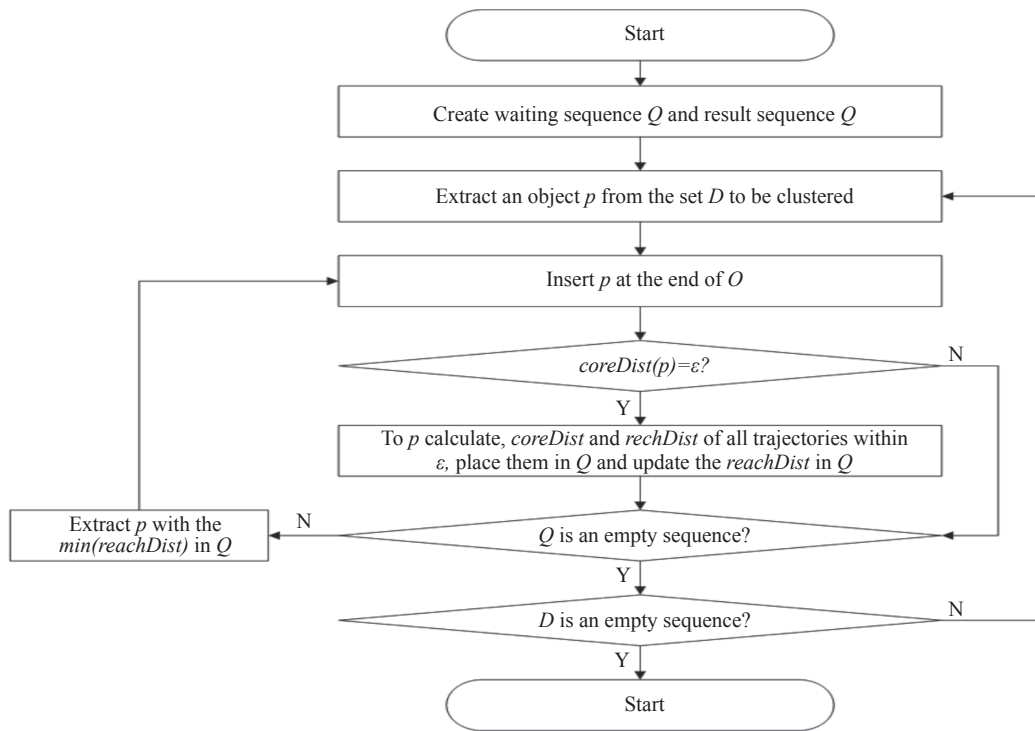
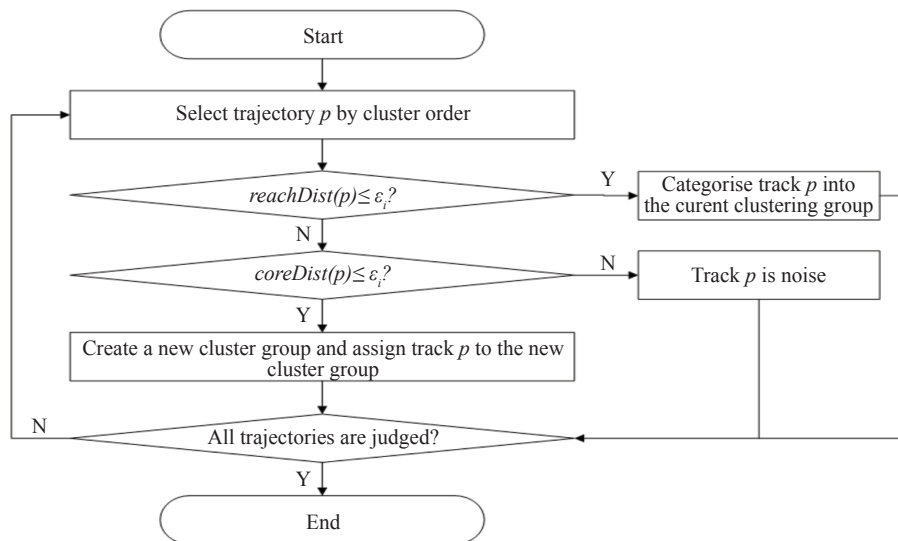


Figure 3 – The details of two stages of OPTICS algorithm



a) Stage 1: Cluster sequence generation



b) Stage 2: Cluster label acquisition

Figure 4 – OPTICS algorithm process

in the  $\varepsilon$ -radius of sample  $x$ , and  $D_F(y, x)$  is the distance from sample  $x$  to sample  $y$ .  $N_\varepsilon^{MinPts}(x)$  is the object in  $x$ 's neighbour that makes  $N(x)=MinPts$  if the  $\varepsilon$ -neighbourhood of  $x$  has more than  $MinPts$ .

The process of cluster label acquisition is shown in Figure 4b. By inputting the clustering threshold  $\varepsilon_p$ , the *reachDist* and *coreDist* of each sample are compared with  $\varepsilon_p$ , and the cluster label of each sample is generated to complete the trajectory clustering.

$$coreDist(x) = \begin{cases} UNDEFINED, & N(x) < MinPts \\ D_F(x, N_\varepsilon^{MinPts}(x)), & N(x) \geq MinPts \end{cases} \quad (1)$$

$$reachDist(y, x) = \begin{cases} UNDEFINED, & N(x) < MinPts \\ \max(coreDist(x), D_F(y, x)), & N(x) \geq MinPts \end{cases} \quad (2)$$

### Determination of the TFP

After clustering of OPTICS, the outer track points on both sides of each cluster are extracted and called side points. Check the number of track points within the radius  $d$  of each side point. If less than the threshold, the side point is removed, otherwise retained. The two lines formed by the retained side points of both sides form the TFP. The side points on both sides of each cluster are matched with distance, and the two side points with the shortest distance are called matching point pairs. The line of the midpoint of all matching point pairs is the centreline of each cluster. This is shown in Figure 5. The centreline is a TFP.

## 2.2 Predicting TFP by using machine learning algorithms

The actual TFP of each historical flight can be obtained directly through Section 2.1. However, due to the influence of weather conditions in the terminal area, the actual TFP may not be the same as the planned TFP, so the weather information on the planned TFP needs to be used as features to predict whether the flight will be rerouted and which route the flight will take after being rerouted.

Machine learning algorithms have a powerful ability to search complex structures and match relationships within objects to predict problems with complex nonlinear features. Figure 6 shows the process of prediction of the TFP using machine learning algorithms. For flights under convective weather conditions, the features are weather information and flight plan data, and the labels are actual TFPs, which are input into the machine learning algorithm. Three machine learning algorithms are used for continuous training to minimise the error between the predicted TFPs and the actual TFPs, and finally, the prediction of the TFPs is completed.

To comprehensively reflect the impact of intensity, altitude, range and duration of convective weather on the selection of the TFP in the terminal area, eight weather features were selected in this paper, including 90<sup>th</sup> percentile *CR*, *maxCR*, 90<sup>th</sup> percentile *ET*, *maxET*, 90<sup>th</sup> percentile *VIL*, *maxVIL*, convective weather coverage and convective weather duration, where *CR*, *ET* and *VIL* are three important weather products, the 90<sup>th</sup> percentile represents the ninetyeth percentile value of the *CR/VIL/ET* on a planned TFP, and *max* represents the maximum value. Convective weather coverage refers to the percentage of convective weather area within the planned TFP, the *VIL* of which is corresponding to NWS Class 3 and above. There are 7 levels of the National Weather Service (NWS). In general, aircrafts are advised to avoid convective weather at NWS level 3 or above [26]. Convective weather duration refers to the duration of the convective weather with a level of NWS 3 or above and the area accounting for 10% or more within the planned TFP.

### Features

In this paper, the planned arrival/departure gate, runway operation direction and the planned IAF point are selected to reflect the flight plan characteristics. After trajectory clustering is achieved by Section 2.1, the planned TFP for each flight is uniquely determined based on the above three flight plan

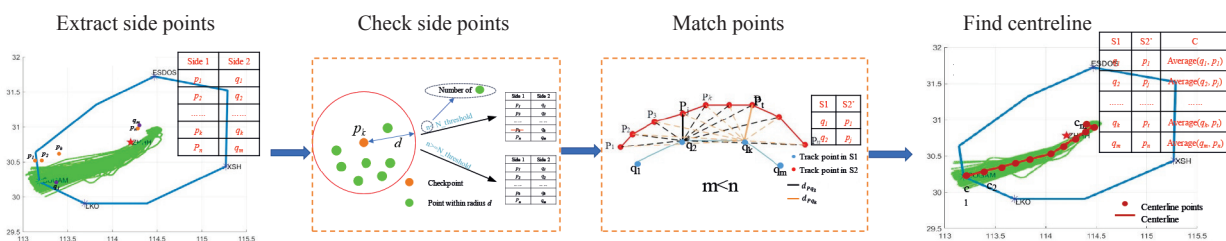


Figure 5 – The diagram of centreline determination

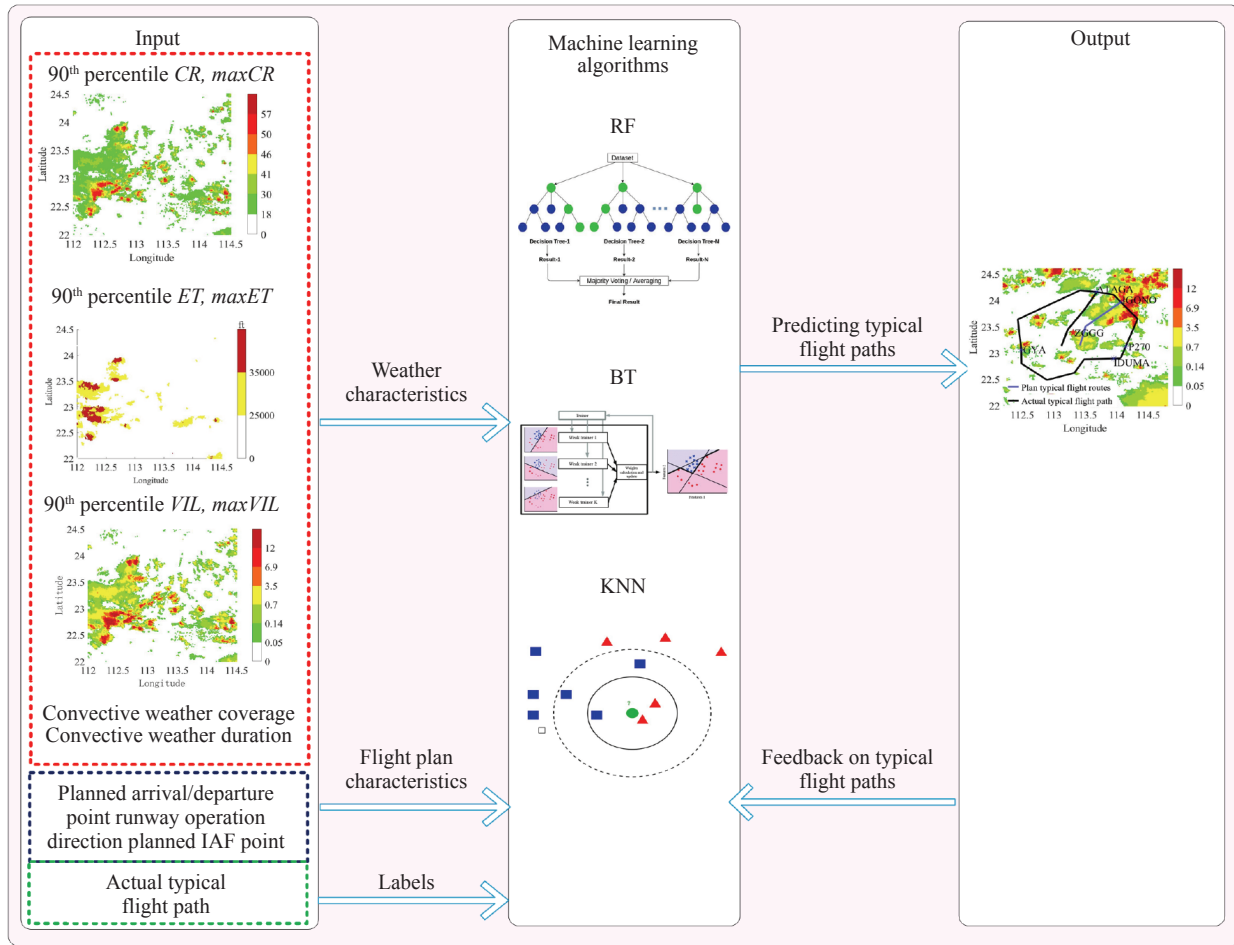


Figure 6 – Process of prediction of the TFP

characteristics. The weather features are obtained within the planned TFP to determine the extent, range and duration that the planned TFP is affected.

**Labels**

The label represents the actual TFP of each flight, where the flights that did not follow any TFP (by ATC) are labelled as 0, while the rest of the flights are labelled as the specific path number (see Figures 12–15).

**Machine learning algorithms**

For machine learning prediction algorithms, the RF uses the decision tree as the base learner and adds random feature selection to increase the robustness and generalisation performance of the prediction. BT is an algorithm that upgrades a weak learner to a strong learner, which is weighted by training several base learners to combine for classification. KNN is a common supervised learning algorithm, which directly obtains the predicted value of the test sample based on the distance between the test sample and

the training samples. The above three algorithms have strong classification ability and applicability, so they are selected for the prediction of the TFPs.

In this paper, we evaluate the prediction algorithm performance for the prediction of TFPs by calculating the accuracy and confusion matrix. The accuracy is calculated as shown in Equation 3, where  $\tilde{y}_i$  is the predicted TFP,  $y_i$  is the actual TFP used by historical flight,  $n$  is the number of samples of the historic flights,  $l$  is a binary variable, 1 when  $y_i$  is the same as  $\tilde{y}_i$ , 0 otherwise. The larger the accuracy, the higher it is, and the better the performance of the prediction algorithm.

$$accuracy = \frac{1}{n} \sum l(y_i = \tilde{y}_i) \tag{3}$$

$$l = \begin{cases} 1, & y_i \text{ is the same as } \tilde{y}_i \\ 0, & \text{otherwise} \end{cases}$$

**2.3 Calculating the availability of the terminal airspace and TFP**

In this paper, terminal airspace availability (TAA) represents the number of flights that the terminal can accommodate under convective weather.

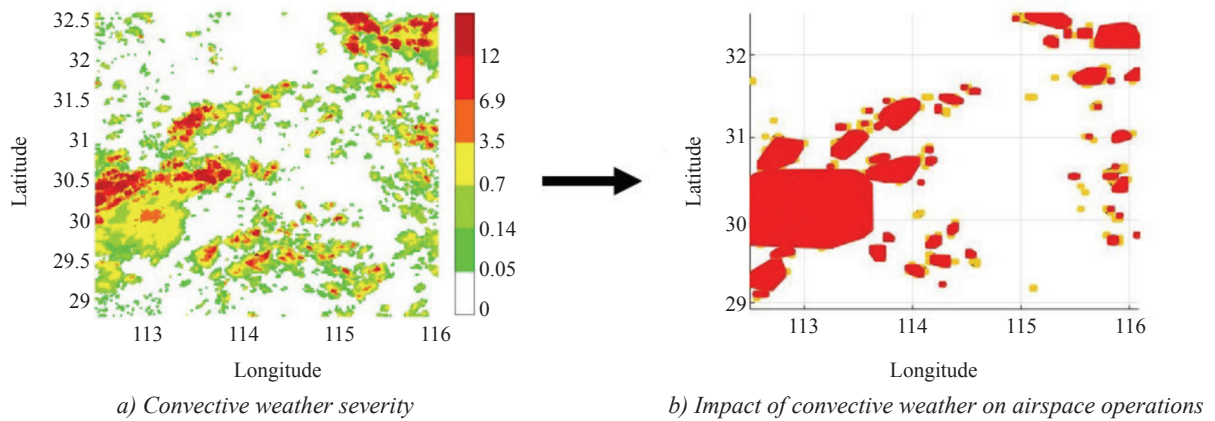


Figure 7 – Convective weather figure

Accordingly, the availability of a TFP (ATFP) refers to the number of flights that can be accommodated by the TFP under convective weather.

The prerequisite of flight path optimisation is to determine the degree and range of the impact of convective weather on airspace operations. According to the literature [27], this paper converts the seven-level weather map of the airspace given by VIL data in Figure 7a into the impact map of convective weather on airspace operations represented by three colours in Figure 7b. The white area in Figure 7b represents the clear weather area where flights are allowed to fly. The yellow area represents the moderate convective weather area where limited flights are allowed to fly. The red area represents the strong convective weather area where flights are prohibited to pass. The red area and yellow area are called convective weather avoid polygon (CWAP). In order to ensure flight safety, a safety margin of 1km is set during the formation of the CWAP.

The TAA [28] is calculated as follows: As shown in Figure 8, assuming that the airport is the origin, the black circle is the boundary of the terminal area, red represents strong convective weather and yellow represents moderate convective weather. A notional route pointing to the boundary of the terminal area is drawn at 1° interval, taking the airport as the origin, and so there are 360 notional routes in a terminal area. When a red block is crossed by a notional route, the score of the notional route is recorded as 0%, a yellow block is crossed, 50% is recorded, and if the notional route does not cross a red block nor a yellow one, a 100% is recorded. For example, the number near the scan lines is the score of the notional route in Figure 8.

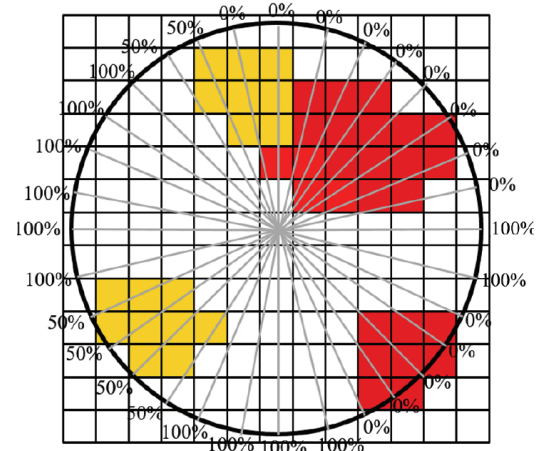


Figure 8 – Schematic diagram for quantifying the severity of convective weather

TAA is finally calculated by Equation 4. The  $F_T$  in Equation 4 is the peak hourly flow rate under clear weather in the terminal area and  $B_s$  is the score of each notional route. In Equation 5,  $ATFP^q$  represents the availability of the  $q^{th}$  TFP, The  $F_R$  is the peak hourly flow rate of the  $q^{th}$  TFP under clear weather and  $N$  is the number of the notional routes contained in the  $q^{th}$  TFP.

$$TAA = F_T \cdot \left( 1 - \frac{\sum_{s=1}^{360} B_s}{360} \right) \tag{4}$$

$$ATFP^q = F_R \cdot \left( 1 - \frac{\sum_{s=1}^N B_s}{N} \right) \tag{5}$$

### 3. MULTI-FLIGHT REROUTING OPTIMISATION

The variables and corresponding meanings of the flight flow optimisation model and the single flight path optimisation model are shown in Table 1.

Table 1 – Variables and meanings

Variables	Meanings
$n$	Total number of planned flights
$x_i$	The binary variable of whether flight $i$ performs radar guidance, 1 if 'yes', 0 otherwise
$x_i^q$	The binary variable of whether flight $i$ flies in the $q^{\text{th}}$ TFP, 1 if 'yes', 0 otherwise
$Q$	Total number of TFPs in the terminal area
$d_i$	The flight path length for flight $i$ by radar guidance
$d_i'$	The flight path length for flight $i$ follows the predicted TFP
$D_i$	The predicted TFP length
$TAA$	Terminal Airspace Availability
$ATFP^q$	The availability of the $q^{\text{th}}$ TFP
$D_{max}$	The maximum permitted flight distance
$CWAP_r$	Red area
$M$	Number of grids of the optimized path during the bidirectional A* algorithm implementation
$CWAP_y$	Yellow area
$R_i$	The flight path of flight $i$
$R_i^o$	The flight path of flight $i$ guided by radar
$R_i^q$	The flight path of flight $i$ follows the predicted TFP

In this paper, the multi-flight rerouting optimisation model is established by bi-level programming. The objective of the upper layer is to maximise the flow in the terminal area, accordingly, the flight flow optimisation model is called. To the single flight path optimisation model, the objective of the lower layer is to minimise the diversion distance of a single flight. In the upper model, while pursuing the maximisation of flow, whether the flight is along the predicted TFP or guided by radar will be determined, that is, the decision variables  $x_i$  and  $x_i^q$  are determined, which is passed to the lower model as the constraint that affects the values of the decision variables of the lower model. In the lower model, while pursuing the optimal flight path, the flight path length can be determined, that is, the decision variables of the lower model  $d_i$  and  $d_i'$  are determined, which is passed to the upper model as the constraint that affects the values of the decision variables of the upper model. This circulation of calculations leads to the final determinations of the optimal solution for the upper and lower layer models.

The reasons for using bi-level programming in this paper are as follows: (1) the intrinsic link between the upper and lower models conforms to the definition of bi-level programming and (2) the transfer of the decision variables between the upper and lower model makes the problem not only clear and easy to understand but also fast and accurate in finding the optimised rerouting path for each flight under the capacity constrain of the TAA and TFP.

The multi-flight rerouting optimisation model is based on the following assumptions: (1) the aircraft for the arrival and departure flight is considered as a point mass; (2) the flight altitude is below 6000m; (3) since the weather data are all distributed along the horizontal direction, the flight path optimisation is set to be two-dimensional; (4) the flight conflicts and the separation between aircraft and terrain obstacles in the terminal area are not considered; (5) the origin and destination points of each flight are fixed when optimising the flight path; (6) the weather data in the middle of the optimisation period is directly used for flight path optimisation because both the optimisation period and the flight time within the terminal area are short.

### 3.1 Multi-flight rerouting optimisation process

According to the calculation of the  $TAA$  and  $ATFP^q$  under convective weather and the prediction of the TFP, the multi-flight rerouting optimisation process is shown in *Figure 9*. The specific steps are described as follows.

*Step 1:* Acquisition of weather and flight plan data for the optimisation period.

*Step 2:* Based on the weather information in the terminal area, *Equations 4 and 5* are used to calculate  $TAA$  and  $ATFP^q$ , and the machine learning algorithms are used to predict the actual TFP. The calculation and prediction results will be regarded as the constraints and initial conditions of the multi-flight rerouting optimisation model.

*Step 3:* The solving algorithm of the flight flow optimisation model is used to obtain the results of whether each planned flight can fly and whether it would adopt radar guidance or the predicted TFP. Then the result is passed to Step 4.

*Step 4:* The path searching algorithm is used to optimise the flight path for each flight, and the optimised flight path is obtained if the maximum number of iterations is reached, otherwise the result of flight path optimisation is passed to Step 3.

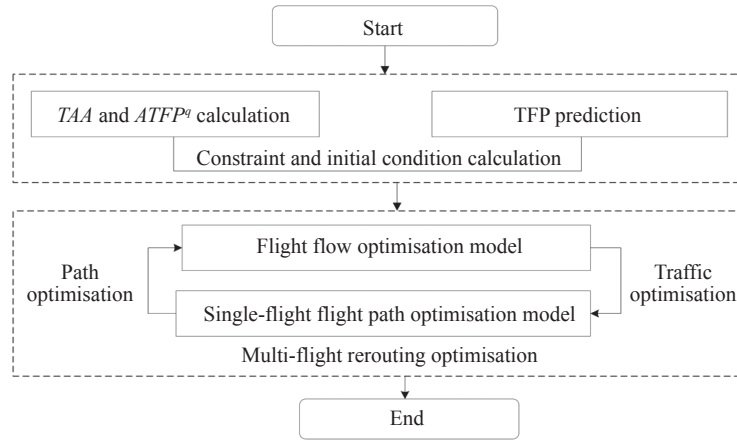


Figure 9 – Multi-flight rerouting optimisation process

### 3.2 Model building

#### Flight flow optimisation model

The flight flow optimisation model is designed to maximise traffic from the perspective of terminal airspace managers under the constraints of TAA, flight distance, etc. The objective function is shown in Equation 6. The flight number of terminal airspace is maximised by giving priority to flights with relatively shorter rerouting distances (obtained by the single flight path optimisation model). Among them,  $D_i/d_i$  and  $D_i/d_i'$  can reflect the cost of flight  $i$  to reroute. When  $x_i$  and the sum of  $x_i^q$  equal 0, flight  $i$  does not plan to fly. It indicates that this flight should delay/cancel its departure, or should be directed to an alternative airport if the flight were already airborne, and this depends on advance time of the weather forecast used in the model. When  $x_i$  equals 1 and the sum of  $x_i^q$  equals 0, flight  $i$  performs radar guidance. When  $x_i$  equals 0 and the sum of  $x_i^q$  equals 1, flight  $i$  follows the predicted TFP. Equations 7 and 8 represent that the flight flow must not exceed the capacity limitation of the terminal area and of the corresponding TFP. Equations 9 and 10 represent that the length of the optimised flight path must not exceed the maximum permitted flight distance. Equation 11 represents that  $x_i$  and  $x_i^q$  can only have at most 1 variable taking the value of 1.

$$\max \sum_{i=1}^n \left( x_i \cdot \frac{D_i}{d_i} + \sum_{q=1}^Q x_i^q \cdot \frac{D_i}{d_i} \right) \quad (6)$$

s.t.

$$\sum_{i=1}^n \left( x_i + \sum_{q=1}^Q x_i^q \right) \leq TAA \quad (7)$$

$$\sum_{i=1}^n x_i^q \leq ATFP^q, \quad q = 1, \dots, M \quad (8)$$

$$d_i x_i \leq D_{\max}, \quad i = 1, \dots, n \quad (9)$$

$$d_i' x_i^q \leq D_{\max}, \quad i = 1, \dots, n, \quad q = 1, \dots, M \quad (10)$$

$$0 \leq x_i + \sum_{q=1}^Q x_i^q \leq 1, \quad i = 1, \dots, n \quad (11)$$

#### Single flight path optimisation model

The single flight path optimisation model is designed to optimise the flight path from the flight operator's perspective based on the constraints of convective weather. The objective function is shown in Equation 12, which aims to minimise the rerouting distance by calculating the diversion between the optimised flight path and the predicted TFP. Equation 13 represents that flights must avoid red areas with severe convective weather, that is, flight paths must not intersect with red areas.

$$\min x_i \cdot (d_i - D_i) + \sum_{q=1}^Q x_i^q \cdot (d_i' - D_i), \quad i = 1, \dots, n \quad (12)$$

s.t.

$$R^i \cap CWAP_r = \emptyset, \quad i = 1, \dots, n$$

$$R_i = \begin{cases} R_i^q, & \text{if } x_i = 1 \\ R_i^q, & \sum_{q=1}^Q x_i^q = 1 \\ UNDEFINED, & \text{otherwise} \end{cases} \quad (13)$$

### 3.3 Solving algorithms

The flight flow optimisation model is solved by the simulated annealing algorithm, and the single flight path optimisation model is solved by the bidirectional A\* algorithm.

#### Simulated annealing algorithm

The simulated annealing algorithm is a heuristic algorithm, which introduces a random factor into the search process and accepts worse solutions with a certain probability when the temperature decreases,

so the simulated annealing algorithm can break through the local optimal solution and find the global optimal solution. The simulated annealing algorithm has good robustness and a simple computational process, which is suitable for solving complex optimisation problems.

Considering the cost of radar guidance and the TFP, the fitness function  $f(X)$  of the simulated annealing algorithm in this paper is the objective function of the upper model, as shown in Equation 6.

The process of the simulated annealing algorithm is shown in Figure 10 and the specific steps are as follows:

*Step 1:* Set the initial temperature  $T$ , the number of iterations  $L$  and the changing rate of temperature  $\alpha$ , and randomly generate the initial solution  $X$ .

*Step 2:* Repeat Step3-Step4 for  $l=1, 2, \dots, L$ .

*Step 3:* Generate the new solution  $X_{new}$  and calculate the difference  $\Delta f$  between  $f(X_{new})$  and  $f(X)$ .

*Step 4:* Accept  $X_{new}$  as the new current solution if  $\Delta f > 0$ , otherwise accept  $X_{new}$  as the new current solution with probability  $\exp(-\Delta f/T)$ .

---

```

X ← SA(T, Tmin, L, α)


---


1: X ← Random();
2: while T > Tmin
3:   for l ← 1 to L do
4:     Xnew ← Random();
5:     Δf = f(Xnew) - f(X);
6:     if Δf > 0
7:       X ← Xnew;
8:     else p = exp(-Δf/T);
9:       if p > Random(0,1)
10:        X ← Xnew;
11:       end if
12:     end if
13:   end for
14:   T ← T × α
15: end while
16: return xi

```

---

Figure 10 – Process of the simulated annealing algorithm

When using the simulated annealing algorithm to implement the fitness function, the initial solution  $X$  is randomly generated and the roulette wheel selection method is used to obtain  $X_{new}$ , and the optimal solution takes the form of binary variables  $x_i$  and  $x_i^q$  for  $n$  flights.

#### Bidirectional A\* algorithm

The A\* algorithm starts searching from the origin point until it reaches the destination point, which is a typical path searching algorithm. The bi-

directional A\* algorithm is an improved algorithm of the A\* algorithm. It searches two paths from the origin point and the destination point: one from the origin point to the destination point and the other from the destination point to the origin point. Finally, it takes the shorter of the two flight paths as the optimised path. The bidirectional A\* algorithm can obtain two optimised flight paths and selects the optimal solution without reducing the computational speed, which is more efficient and accurate.

The bidirectional A\* algorithm uses the full graph information to perform a directed and purposeful search. The algorithm will perform path searching with an evaluation function  $F$ , where  $G$  is the Euclidean distance from each point to the origin point and  $H$  is the Manhattan distance from each point to the destination point, as shown in Equations 14–16.

$$F = G + H \quad (14)$$

$$G = \sqrt{(X_{Start} - X_p)^2 + (Y_{Start} - Y_p)^2} \quad (15)$$

$$H = |X_{End} - X_p| + |Y_{End} - Y_p| \quad (16)$$

The process of the bidirectional A\* algorithm is shown in Figure 9 and the specific steps are as follows:

*Step 1:* Add the origin point  $P_{Start}$  to the open list.

*Step 2:* Repeat the following process:

- Iterate through the open list to find the path point  $P_{Temp}$  with the smallest  $F$  and regard it as the current path point to be processed.
- Move  $P_{Temp}$  to the close list.
- Judge and process each of the 8 neighbouring points (centre of a grid in this paper, the size of the grid is  $0.01 \times 0.01^\circ$ , which is  $1 \text{ km} \times 1 \text{ km}$ , the basic unit of meteorological information storage)  $P$  of  $P_{Temp}$ : if  $P$  is not reachable or  $P$  is in the close list, do not process it. If  $P$  is not in the open list, set  $P_{Temp}$  as its father node and add  $P$  to the open list. If  $P$  is already in the open list, use  $G$  to check whether the path to  $P$  via  $P_{Temp}$  is better. If it is, update its father node to  $P_{Temp}$ , and recalculate its  $G$  and  $F$  value.
- Determine whether to stop the path searching: stop searching when the destination point  $P_{End}$  is added to the open list, or the search for  $P_{End}$  with an empty open list has failed.

*Step 3:* Move along the father node of each path point from  $P_{End}$  to  $P_{Start}$  as the rerouting path.

*Step 4:* Swap  $P_{Start}$  and  $P_{End}$ , and perform Step 1 to Step 3 at the same time.

---

```

Route ← A*(PStart, PEnd)


---


1: open list ← AddNode(PStart);
2: while PEnd not in open list or open list not empty
3:   PTemp ← Search(open list);
4:   close list ← Remove(PTemp);
5:   for (each successor node P of PTemp)
6:     if P unreachable or in close list
6:       skip;
7:     end if
8:     if P not in open list
9:       PTemp ← FatherNode(P);
10:    else if GPTemp < GPold
11:      PTemp ← FatherNode(P);
12:      FP ← Calculate(F);
13:      GP ← Calculate(G);
15:    end if
14:  end if
15:  end for
16: end while
17: return Route


---



```

Figure 11 – Process of the bidirectional A\* algorithm

There are five aspects that need to be explained. Firstly, the  $P_{Start}$  and  $P_{End}$  of the predicted arrival TFP are set as the arrival point and IAF respectively, and the  $P_{Start}$  and  $P_{End}$  of the predicted departure TFP are set as the first turn point after departure (if any, otherwise the airport) and departure gate respectively. The purpose of this is to align the flight trajectory with the runway after take-off or during the final approach.

Second,  $P_{Start}$  and  $P_{End}$  of the predicted TFP may be located within the convective weather area. For arrival flights, if there is severe convective weather in ‘a certain range’ of  $P_{Start}$  and  $P_{End}$ ,  $P_{Start}$  will be moved 1 km at a time in both directions along the boundary of the terminal area.  $P_{End}$  is searched within a limited range near the original  $P_{End}$  (IAF) until  $P_{End}$  meets the requirement of no severe convective weather in ‘a certain range’. If  $P_{End}$  cannot be searched, then initial  $x_i$  and  $x_i^q$  are set to 0. For departure flights, the determination of  $P_{Start}$  and  $P_{End}$  corresponds to the determination of  $P_{End}$  and  $P_{Start}$  of arrival flights.

Third, if ‘a certain range’ mentioned in the second aspect is set too large, the conditions for obtaining the origin and destination points are too harsh. If the range is too small, there is a possibility that the origin and destination points are surrounded by convective weather, and the optimised path cannot be found. In this paper, ‘a certain range’ refers to 1 km (8 neighbouring grids) around  $P_{Start}$  and  $P_{End}$ .

Fourth, to ensure that  $P_{End}$  of arrival flights is in the terminal area and not too far away from IAF, ‘a limited range’ mentioned in the second aspect is set to 3 km (48 grids of 3 circles around the original  $P_{End}$ ). The initial direction of the search is the direction of the line between the original  $P_{Start}$  and  $P_{End}$ , which means for the same search radius, first searching the point on the line and then traversing clockwise through the points around the original  $P_{End}$  from the first searching point until  $P_{End}$  meets the requirement of no severe convective weather in ‘a certain range’. When the search point is outside ‘a limited range’ or outside the terminal area or in other unreasonable areas, the search stops to ensure path validity.

Finally, the two-direction search mentioned in Section 2 leads to two possible endpoints. In the paper, one of the two endpoints is selected if the path it forms is less affected by the weather. Otherwise, the endpoint is selected which is further away from the nearest gate of arrival or departure than the other, in order to minimise the impact on the flight operation.

## 4. RESULT

In this paper, we selected flight data from 3 August to 31 August 2018, including the flight plan, historical radar trajectory and weather data. The flight plan data include flight number, aircraft type, departure airport, arrival airport, planned path and other information. Historical radar trajectory data is updated at a rate of 8 seconds, including time, flight number, longitude, latitude and other information. Weather data includes CR, ET and VIL, with an update rate of 6 minutes and stored in the form of  $0.01^\circ \times 0.01^\circ$  (longitude  $\times$  latitude). There are 10,551 arrival flights and 13,041 departure flights of the Guangzhou terminal area, while there are 6,345 arrival flights and 6,595 departure flights of the Wuhan terminal area.

### 4.1 TFP based on the OPTICS Algorithm

According to Section 2.1, the historical radar tracks of 10,551 arrival and 13,041 departure flights in the Guangzhou terminal area and 6,345 arrival and 6,595 departure flights in the Wuhan terminal area were clustered based on OPTICS algorithm [30] to obtain TFPs. Figures 12–15 show the clustering results of the typical arrival and departure flight paths. For example, the arrival radar

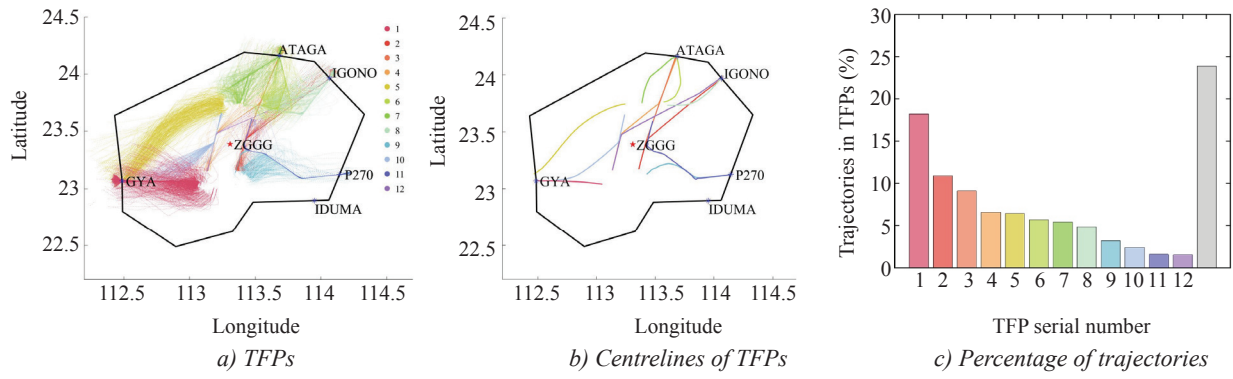


Figure 12 – Clustering results of arrival flights of the Guangzhou terminal area

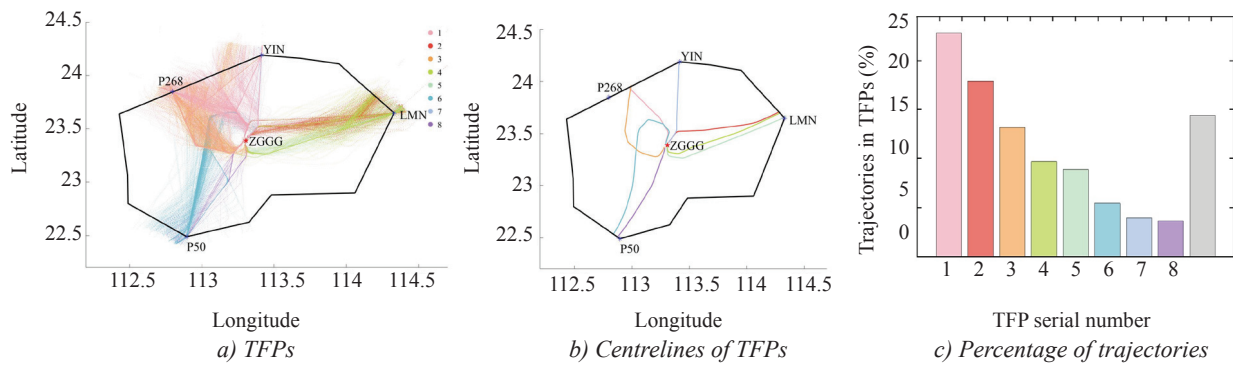


Figure 13 – Clustering results of departure flights of the Guangzhou terminal area

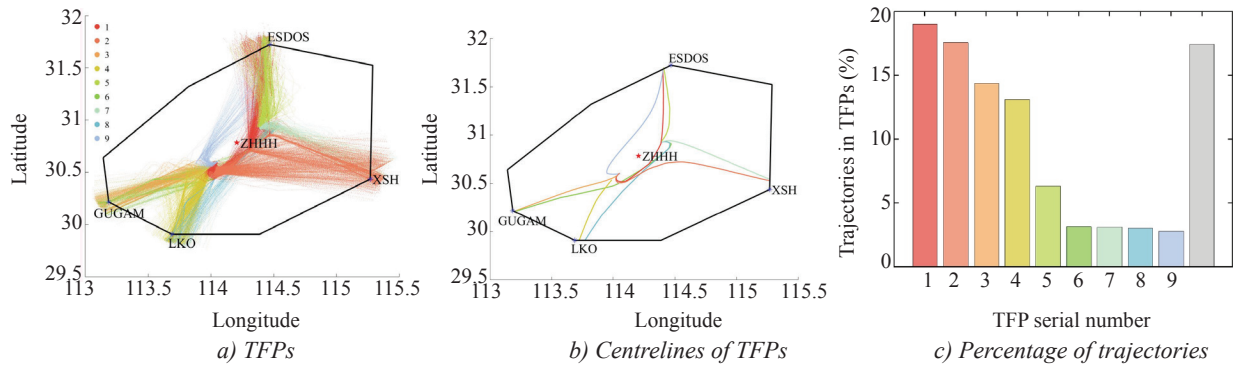


Figure 14 – Clustering results of arrival flights of the Wuhan terminal area

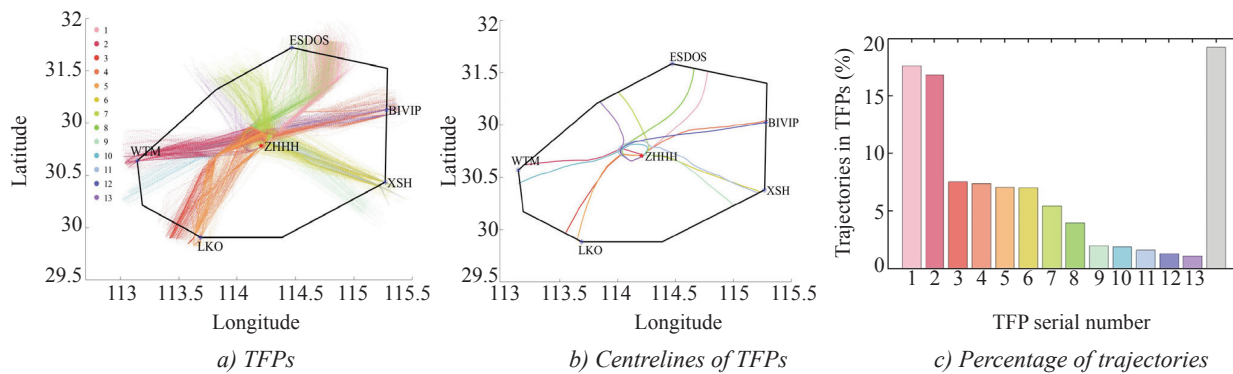


Figure 15 – Clustering results of departure flights of the Wuhan terminal area

trajectory clustering results in the magenta colour at GYA of *Figure 12a* correspond to the trajectories centreline of the TFP in the magenta colour at GYA of *Figure 12b*, and the No. 1 TFP of *Figure 12c*. *Figures 12a–15a* show the trajectory clustering results of arrival and departure flights of the Guangzhou and Wuhan terminal area. The black polygon in the figure is the terminal area boundary, the blue asterisk point is the arrival or departure gate, the red pentagram is the location of the airport and different colours represent different TFPs. The number of TFPs of Guangzhou arrival flights, Guangzhou departure flights, Wuhan arrival flights and Wuhan departure flights is 12, 7, 9 and 13 respectively. Referring to *Figure 2*, the number and location of TFPs of arrival and departure in the two terminal areas are indeed different from the published arrival and departure paths, and it was also verified with local controllers in both terminal areas.

*Figures 12b–15b* show the centreline of the TFPs, indicating the information of the origin point, destination point and trend. *Figures 12c–15c* show the percentage of trajectories in each TFP, with the number of flights (by radar guidance) that are not clustered into any of the TFPs in grey. As seen in *Figures 12c–15c*, the number of flights at each arrival and departure gate with different runway operating directions varies, which results in different percentages of trajectories included in each TFP.

In addition, the percentage of flights marked in grey is also different for the Guangzhou and Wuhan terminal area. Most of these flights performed radar guidance due to convective weather, which indicates the difference in frequency, range and intensity of convective weather, and the variation in the pilots' flight strategies and habits of the two terminal areas.

## 4.2 Algorithm determination of the TFP prediction

For the prediction of the TFPs, 5,405 arrival flights and 3,697 departure flights of the Guangzhou terminal area and 1,685 arrival flights and 1,823 departure flights of the Wuhan terminal area under convective weather were selected as the training samples in this paper.

The parameters of the prediction algorithm of the TFP are set as follows: the base learner of the RF is the decision tree, the number of learners is 30; the base learner of the BT is the decision tree, the integration method is Adaboost, the number of

learners is 30, the maximum number of splits is 20 and the learning rate is 0.1; the k value of KNN is 3, the distance metric is Euclidean distance, the distance weight is equidistant and the input features are normalised before prediction. The ten-fold validation method is used in the calculation and the final accuracy of each algorithm is averaged over ten experiments to evaluate the performance of each algorithm.

Based on *Equation 3*, *Figure 16* shows the comparison of the prediction accuracy of the three machine learning algorithms for typical arrival and departure paths of the Guangzhou and Wuhan terminal area. The RF shows the best performance on all four datasets, ranging 2–8% higher than the BT and KNN algorithms, indicating the superior performance of the RF in the prediction of the TFPs.

*Figures 17 and 18* show the prediction results of the TFPs using the RF algorithm in the Guangzhou and Wuhan terminal area. The results show that the percentage with prediction accuracy over 90% are 53.8% (No. 0, 4, 5, 6, 7, 10, 11 TFP), 50% (No. 0, 1, 4, 7 TFP), 40% (No. 0, 5, 6, 9 TFP), 21.4% (No. 0, 4, 5 TFP). The percentage with prediction accuracy over 75% are 61.5% (No. 0, 1, 4, 5, 6, 7, 10, 11 TFP), 62.5% (No. 0, 1, 3, 4, 7 TFP), 70% (No. 0, 1, 2, 5, 6, 8, 9 TFP) and 35.7% (No. 0, 1, 4, 5, 8 TFP). For flights with a label of 0 (Radar guidance), the prediction accuracy exceeded 92% on all four datasets. The most important reason for the prediction error is that the number of flights using some TFPs under convective weather is low, resulting in the training samples of these TFPs being low. For example, No.11 to No.13 TFPs in *Figure 18b* have less than 10 samples. It can be seen that with sufficient sample size, the RF algorithm can predict with high accuracy whether a flight performs radar guidance and which TFP to fly under convective weather conditions. Therefore, the RF algorithm is chosen to predict the TFP in this paper.

## 4.3 Case study

### *Convective weather condition*

*Figure 19* shows the radar trajectories of the Guangzhou terminal area from 11:30:00–12:30:00 on 19 August 2018, and the Wuhan terminal area from 11:30:00–12:30:00 on 31 August 2018, respectively. The base map is VIL, reflecting the severity and range of convective weather. As seen in *Figure 19a*, there is a larger area of convective

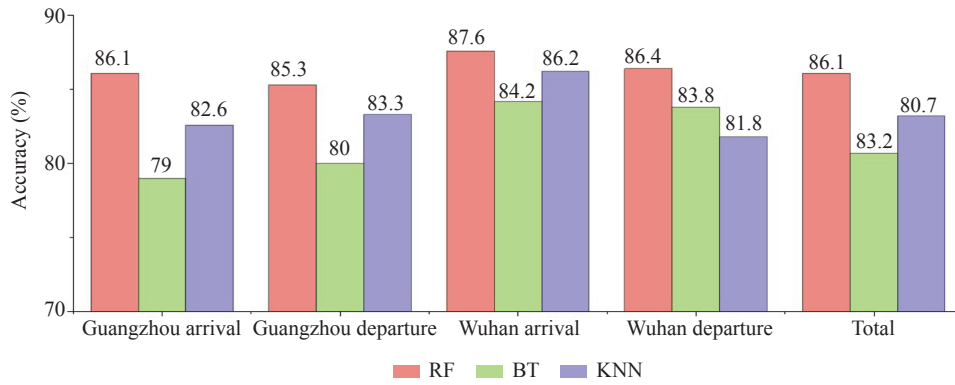


Figure 16 – Comparison of prediction accuracy of the TFPs

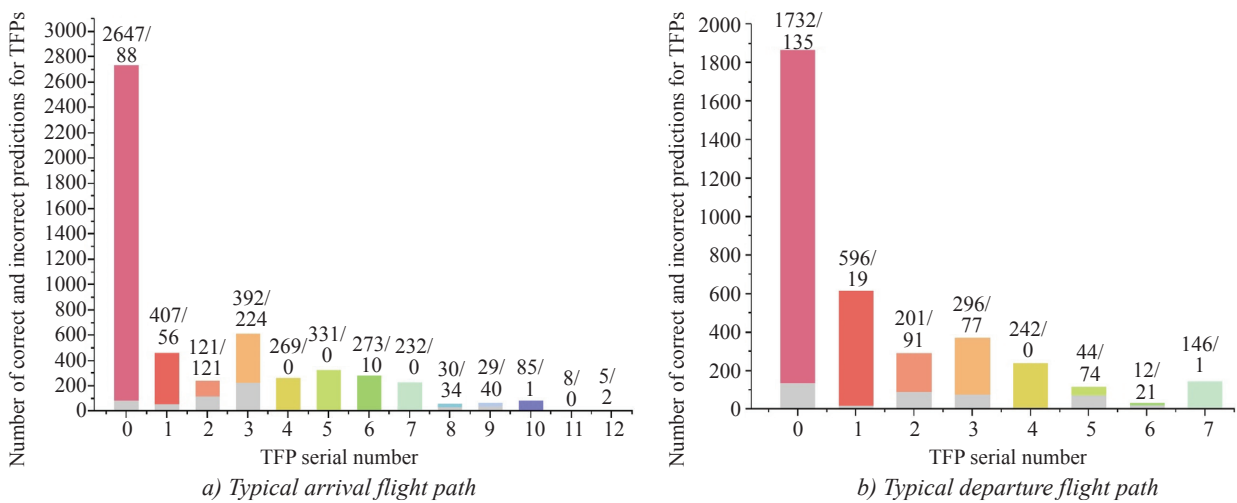


Figure 17 – Prediction results using the RF algorithm in Guangzhou terminal area

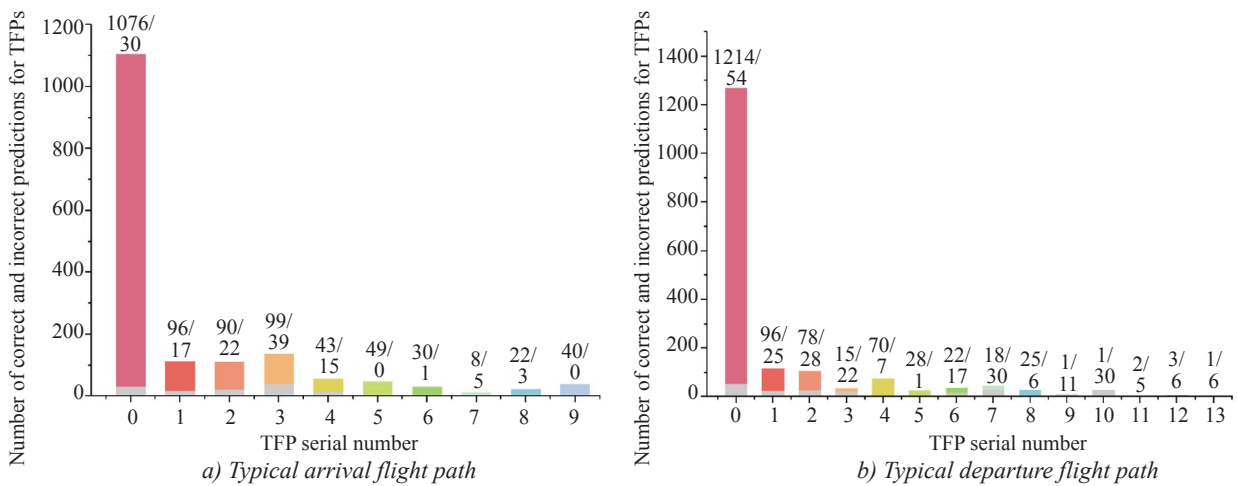


Figure 18 – Prediction results using the RF algorithm in Wuhan terminal area

weather on the west side of the Guangzhou terminal area and a smaller area of convective weather on the north and southeast sides, so the number of flights in the west direction is low, and most flights complete their arrival and departure from the north and east di-

rections. As seen in Figure 19b, there is a large area of convective weather on the west side of the Wuhan terminal, and there are several scattered small areas of convective weather on the northwest side, so most of the flights completed their arrival and departure from

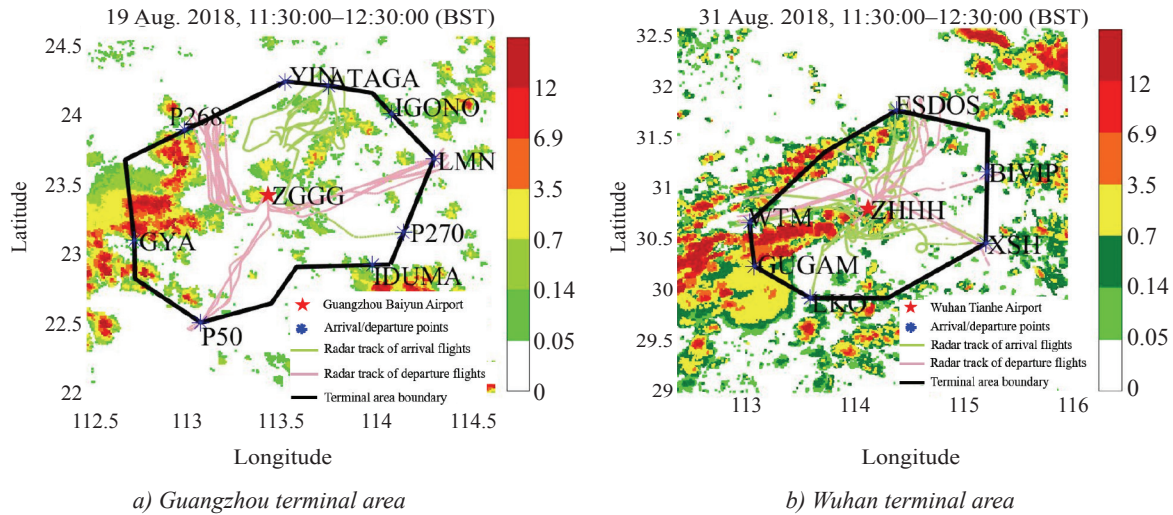


Figure 19 – Radar trajectories and VIL information

the north and southeast directions, and the flights on the west side completed their arrival and departure from the interval of convective weather areas.

*The calculation results of TAA and ATFP*

Table 2 shows the planned flight number, actual flight number, the TAA and ATFP for the Guangzhou and Wuhan terminal area during the period of the case study. The planned flight number of the Guangzhou and Wuhan terminal area are 51 and 34. The historical actual flight numbers are 42 and 28 because of convective weather. The TAA is calculated using Equation 4 to be 46 and 31, respectively. According to Equation 5, the ATFP of each arrival and departure is affected then and the total ATFP in the Guangzhou and Wuhan terminal areas is also calculated.

*The prediction results*

As shown in Figure 6, 8 weather features including the 90<sup>th</sup> percentile CR, maxCR, 90th percentile ET, maxET, 90<sup>th</sup> percentile VIL, maxVIL, convective weather coverage and convective weather duration, as well as three flight plan features including the runway operation direction, planned arrival and departure gates, and planned IAF points are put into prediction model obtained by the RF algorithm to predict the TFP of each flight.

Tables 3 and 4 show the basic flight information and predicted TFPs for 51 flights of the Guangzhou terminal area and 34 flights of the Wuhan terminal area, respectively.

Tables 3 and 4 show the basic flight information and predicted TFPs. In Table 3, the number of flights that are predicted correctly is 45, and incorrectly six. These six flights were all planned to arrive from IGONO, but actually arrived from ATAGA. The actual TFP is No.6 and the predicted TFP is No.8. The reason for the error is the relatively weak convective weather conditions on the planned TFP of the six flights during the prediction period, while the actual situation is that the pilots completed the arrival from ATAGA for flight safety and traffic control reasons. In Table 4, the number of flights that are predicted correctly is 32, and incorrectly two. These two flights are predicted to depart from the No.3 TFP at LKO and are actually performed by radar guidance. The reason for the error is that although the convective weather on the No.3 TFP was strong during the prediction period, the convective weather only existed in part of the TFP and did not block the cross-section of the path, so the flights could still fly as planned. But in reality, the pilots took radar guidance to complete the departure for safety reasons. It seems that both errors can be related to the

Table 2 – Traffic count of Guangzhou and Wuhan terminal area

	Guangzhou Terminal Area	Wuhan Terminal Area
Planned/Actual/TAA	51/42/46	34/28/31
ATFP	(Arrival No. 6: 7; Arrival No. 8: 6; Arrival No. 11: 2; Departure No. 3: 1; Departure No. 4: 9; Departure No. 7: 6;)	(Arrival No. 1: 7; Arrival No. 2: 2; Departure No. 1: 6; Departure No. 4: 1; Departure No. 9: 3;)

Table 3 – Basic flight information and predicted TFPs (Guangzhou Terminal Area)

Flight number	Planned arrival and departure gates	Arrival/Departure	Actual TFP	Predicted TFP	Flight number	Planned arrival and departure gates	Arrival/Departure	Actual TFP	Predicted TFP
CSN6916	ATAGA	Arrival	6	6	CSN3958	IGONO	Arrival	6	8
CSH9304	LMN	Departure	4	4	CSN3539	LMN	Departure	4	4
CES5321	GYA	Arrival	0	0	CDG1170	LMN	Departure	4	4
CSN6341	ATAGA	Arrival	6	6	CSN3103	YIN	Departure	3	3
CCA4306	YIN	Departure	3	3	CES5303	IGONO	Arrival	6	8
CSZ9691	YIN	Departure	3	3	CSZ9860	IGONO	Arrival	6	8
CSN3415	VIBOS	Departure	7	7	CSZ9956	IGONO	Arrival	6	8
CES2301	GYA	Arrival	0	0	CSN6790	VIBOS	Departure	7	7
CBJ5737	GYA	Arrival	0	0	CES5734	VIBOS	Departure	7	7
CSN3245	YIN	Departure	3	3	CSN3400	GYA	Arrival	0	0
CSN3624	ATAGA	Arrival	6	6	CSN3534	IGONO	Arrival	6	8
CSN3000	ATAGA	Arrival	6	6	CSN3950	GYA	Arrival	0	0
CSN6563	YIN	Departure	3	3	CDG4898	LMN	Departure	4	4
CSN355	YIN	Departure	3	3	CES5258	LMN	Departure	4	4
CSN6742	VIBOS	Departure	7	7	CSN3499	VIBOS	Departure	7	7
CSZ9190	ATAGA	Arrival	6	6	CSZ9442	GYA	Arrival	0	0
CSN3883	LMN	Departure	4	4	CES2551	ATAGA	Arrival	6	6
CHH7310	YIN	Departure	3	3	CHH7838	YIN	Departure	3	3
CSN3517	LMN	Departure	4	4	CXA8323	SHL	Arrival	11	11
CQN2324	YIN	Departure	3	3	CSN3443	YIN	Departure	3	3
CSN3812	SHL	Arrival	11	11	CSN3404	GYA	Arrival	0	0
CSN3778	IGONO	Arrival	6	8	CCA4335	ATAGA	Arrival	6	6
CES5252	YIN	Departure	3	3	CSN3327	VIBOS	Departure	7	7
CES5182	YIN	Departure	3	3	CCA1352	YIN	Departure	3	3
CCA1318	YIN	Departure	3	3	CSH9310	LMN	Departure	4	4
CXA8386	LMN	Departure	4	4					

fact that optimised trajectories are riskier than the actual practice. This suggests that people prefer to take safer paths conservatively, which would lead to more regulated workloads and flight times.

#### The multi-flight rerouting optimisation results

After obtaining the prediction results of the TFPs, refer to Figures 12b-15b to obtain the length of the predicted TFP for each flight and set the initial condition. In Equation 6,  $d_i$  and  $d_i'$  are equal to  $D_i$  for flights with non-zero predicted value, otherwise,  $d_i$  and  $d_i'$  are equal to  $99 \cdot D_i$ . The reason for this setting is that under the limitation of TAA, the upper model gives priority to the flights predicted to have specific TFPs and then arranges the flights

to perform radar guidance so that the flight flow in the terminal area can be maximised. The solution is carried out by Equations 6–15 with the objectives of maximising the flight flow and minimising the flight rerouting distance. The flight flow optimisation model uses the simulated annealing algorithm, and the parameters are set as follows: the initial temperature  $T$  is 1000, the number of iterations  $L$  is 50, the temperature change rate  $\alpha$  is 0.99 and  $T_{min}$  is 1. The maximum number of iterations is 50.

In this paper, a computer configured with an i7-9750H CPU processor and 16GB RAM is used to solve the model by using the Matlab software. The computation times for the Guangzhou and Wuhan

Table 4 – Basic flight information and predicted TFPs (Wuhan terminal area)

Flight number	Arrival and departure gates	Arrival/Departure	Actual TFP	Predicted TFP	Flight number	Arrival and departure gates	Arrival/Departure	Actual TFP	Predicted TFP
LKE9958	WTM	Departure	0	0	CSZ9832	XSH	Departure	9	9
CES2543	BIVIP	Departure	4	4	CES2485	WTM	Departure	0	0
CHH7875	ESDOS	Arrival	1	1	CHH7789	LKO	Arrival	0	0
HXA2807	ESDOS	Arrival	1	1	CBJ5385	ESDOS	Arrival	1	1
CES2460	WTM	Departure	0	0	CSN3118	ESDOS	Arrival	1	1
CSC8219	WTM	Departure	0	0	CES2478	LKO	Arrival	0	0
JOY1527	XSH	Arrival	2	2	CES9735	GUGAM	Arrival	0	0
CBJ5137	GUGAM	Arrival	0	0	CCA8222	GUGAM	Arrival	0	0
CES2473	ESDOS	Arrival	1	1	CSN3705	LKO	Arrival	0	0
CBJ5286	LKO	Departure	0	3	CSN6513	ESDOS	Departure	7	7
CSZ9127	ESDOS	Departure	7	7	CSN3448	GUGAM	Arrival	0	0
CUH2517	ESDOS	Arrival	1	1	CSN6568	ESDOS	Departure	7	7
CXA8338	XSH	Departure	9	9	GCR7591	ESDOS	Departure	7	7
CSN6608	ESDOS	Arrival	1	1	CCA8258	LKO	Arrival	0	0
RLH5302	ESDOS	Departure	7	7	CES2506	XSH	Arrival	2	2
LKE9891	GUGAM	Arrival	0	0	CSN3663	ESDOS	Departure	7	7
CHH7187	XSH	Departure	9	9	CSC8725	LKO	Departure	0	3

terminal area are 186 seconds and 158 seconds, respectively, which are shorter than the update time of weather data (6 minutes) and meet the computation speed requirements for practical applications. Figure 20 illustrates part of the planned TFPs of the Guangzhou and Wuhan terminal area and Figure 21 illustrates corresponding flight path optimisation results of the Guangzhou and Wuhan terminal area. As can be seen from Figures 20 and 21, large areas of severe convective weather are present to the west of the Guangzhou and Wuhan terminal area, and the optimised rerouting allows for a shorter rerouting distance to complete the arrival and depart-

ture while avoiding the convective weather area, such as the brown line in Figure 21a and the dark green line in Figure 21b. In areas where convective weather is weak or does not exist, TFPs are used as flight paths, such as the dark green in Figure 21a and the brown line in Figure 21b. Thus the effectiveness of the multi-flight rerouting optimisation model is demonstrated.

#### 4.4 Analysis

Table 5 shows the calculation results of the optimised path in the Guangzhou and Wuhan terminal area. After the optimisation, the flight flow in

Table 5 – Comparison of historical flights and optimization results of the Guangzhou/Wuhan terminal area

	Historical flights	Optimization results	Compared to historical flight (%)
Total flights number	42/28	46/31	9.5/10.7
Number of flights crossing moderate convective weather areas	5(4)/3(0)	8(6)/7(5)	60/133.3
Number of flights flying on planned TFPs	10/7	14/9	40/28.6
Flight distance in moderate convective weather areas (km)	28/35	55/39	96.4/11.4
Total length of the flight path (km)	5732.2/4369.6	3920.7/3037.5	-31.6/-30.5

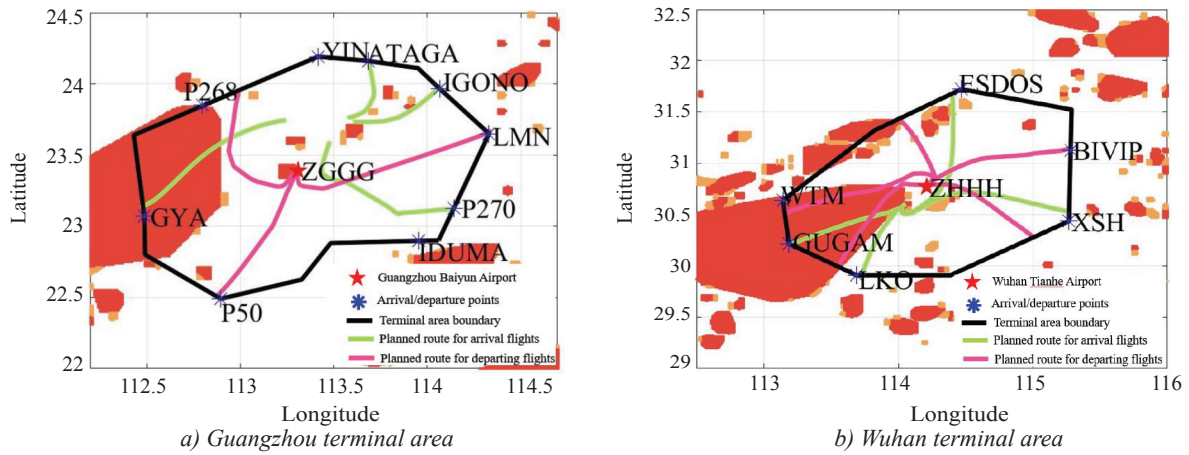


Figure 20 – Planned TFP

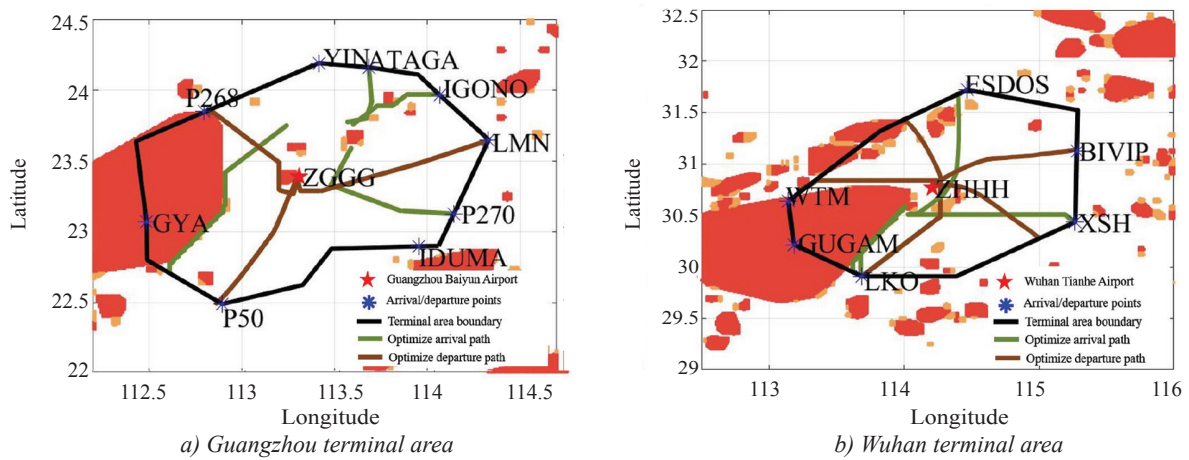


Figure 21 – Flight path optimisation results

the Guangzhou and Wuhan terminal area increased by 9.52% and 10.71%, and the number of flights crossing moderate convective weather in the terminal area increased by 60% and 133.3%, where the number in brackets is the number of flights crossing moderate convective weather on TFPs. Flights flying on planned TFPs increased by 40% and 28.6% respectively. The three indicators above illustrate the significant increase in effective airspace utilisation during convective weather conditions. The flight distance in moderate convective weather areas increased by 96.4% and 11.4% and the total length of the flight path is reduced by 31.6% and 30.5% respectively. These two indicators show that while avoiding areas of strong convective weather, the total length of the flight path is reduced, flight safety is ensured and flight cost is saved.

There are four possible reasons for these results. The most important one is the model itself can well solve the optimisation of flight path under convective weather, which improves the utilisation of airspace in

the terminal area and reduces of flight distance. The second is conservative flight during actual operation. In order to achieve safer operation under convective weather, the airspace capacity under moderate convective weather was underutilised by historical flights. Many flights avoided moderate convection weather on TFPs and other airspaces in the terminal areas and operated in airspace without convective weather by radar guidance. The cost of this conservative operation approach to flight safety is a longer total flight path length. The third possibility is that the safety margin of CWAP used in this paper is set relatively small. If the safety margin is set large, multiple CWAPs would be connected, and the airspace used for rerouting would be small, the rerouting distance would be increased, but the safety of flight operation would also be increased. On the other hand, if the safety margin is set small or even if there is none, the airspace for rerouting would be increased, but the rerouting would be close to the convective weather, which would increase the operational risk of the flight. In this paper, a safety margin of 1 km is

adopted as a compromise. The ways to set the margin of the CWAP according to the wind in the terminal area should be studied in the future. Not only that, these results are also related to the cases we chose. It would be different in the case of different terminal areas under different convective weather at different times and different controllers and pilots. But it can be expected that the trend, i.e. that the TAA will increase and total flight distance will decrease, will always be present by taking advantage of the availability of moderate convective weather.

## 5. CONCLUSION

In this paper, we use TFPs instead of flight procedures to reflect flight patterns within the terminal area and carry out the prediction of the TFPs by RF, BT, and KNN algorithms. Then we establish a multi-flight rerouting optimisation model and take the Guangzhou and Wuhan terminal area as the research objects to complete flight path optimisation. The conclusions are as follows:

- 1) In the prediction algorithm determination of the TFPs, the accuracy of the RF algorithm in Guangzhou arrival dataset, Guangzhou departure dataset, Wuhan arrival dataset and Wuhan departure dataset are 90.7%, 88.4%, 92.2% and 86.4% respectively, with an average value of 89.0%, which is the best of the three algorithms.
- 2) The TFPs of 51 and 34 flights during the designated time of the Guangzhou and Wuhan terminal area are predicted by the RF algorithm. The number of prediction errors is 6 and 2 respectively, which verifies the feasibility and effectiveness of the prediction of the TFPs;
- 3) Taking TAA and A\* under convective weather conditions as constraints and prediction results of the TFPs as initial conditions, the simulated annealing algorithm and bidirectional A\* algorithm are used to solve the upper and lower layers of the multi-flight rerouting optimisation model. The computation times are 186 seconds and 158 seconds, respectively, which are less than the update time of weather data 6 minutes, meeting the computational speed requirements of flight path optimisation under convective weather conditions.
- 4) Compared to the optimisation results with the historical flights, the total length of the flight path of the Guangzhou and Wuhan terminal area decreases while the flight flow increases under the condition of meeting the TAA restrictions and en-

suring flight safety, demonstrating reasonable and efficient flight path optimisation under convective weather conditions.

The optimised rerouting realised by the multi-flight rerouting optimisation model can not only avoid convective weather to ensure flight safety but also increase the airspace availability in the terminal area, reduce flight delay and improve airspace utilisation.

In this paper, the safety margin of the CWAP is set to 1 km, which is also one of the reasons for the rerouting result. The ways to set the safety margin according to the weather information such as wind direction and the influence of the set size on the rerouting effect will be the focus of future research. In addition, flight rerouting optimisation for avoiding convective weather in the terminal area is realised without considering the airspace environment, such as obstacles and three areas (prohibited area, restricted area, danger area) in the terminal area, which will directly affect the results of rerouting optimisation. This would also be the focus of the next steps in future research work.

王世锦, 博士<sup>1</sup> (通讯作者)

电子邮箱: shijin\_wang@nuaa.edu.cn

段荣荣, 硕士研究生<sup>1</sup>

电子邮箱: duanrongrong@nuaa.edu.cn

储洁雯, 硕士研究生<sup>1</sup>

电子邮箱: 421707865@qq.com

李家豪, 职员<sup>2</sup>

电子邮箱: 920728951@qq.com

杨宝田: 硕士研究生<sup>1</sup>

电子邮箱: 1756495209@qq.com

<sup>1</sup> 南京航空航天大学民航学院:

江苏省南京市江宁区将军大道29号, 210016

<sup>2</sup> 中兴通讯股份有限公司:

江苏省南京市雨花台区软件大道50号, 210012

终端区对流天气下基于典型飞行路线的航班路径优化

摘要:

随着航班量的快速增长, 对流天气对终端区航班运行的影响愈加严重。本文以典型飞行路线替代飞行程序作为终端区内航班的常规飞行路线, 基于天气特征和飞行计划特征, 通过随机森林(*Random Forest, RF*)、提升树(*Boosting Tree, BT*)和K最近邻(*K-Nearest Neighbour, KNN*)算法预测航班典型飞行路线, 构建包含上层飞行流量优化模型和下层单航班飞行路径优化模型的双层多航班改航路径优化模型, 分别使用模拟退火算法和双向A\*算法实现上下层模型的求解。本文采用广州白云机场(*ZGGG*)和武汉天河机场(*ZHHH*)终端区进行案例分析, 相较于BT和KNN, RF算法有着更好的预测航班典型飞行路线性能; 与历史雷达轨迹相比, 航班路径优化结果表

明, 对于广州终端区, 在满足终端区空域可用性的限制条件下, 飞行流量增加, 飞行距离减少, 有效提高了终端区内的运行效率。

关键词:

终端区; 对流天气; 典型飞行路线;  
终端区空域可用性; 路径优化

## REFERENCES

- [1] Department of Development Planning. *Statistical bulletin on the development of the civil aviation industry from 2017-2021*. Civil Aviation Administration of China; 2018-2022.
- [2] Civil Aviation Administration of China. *Civil aviation air traffic management rules*. Civil Aviation Administration of China. Report number: 30, 2017.
- [3] Campbell S, Matthews M, Delaura R. Air traffic decision analysis during convective weather events in arrival airspace. *AIAA*. 2012. doi: 10.2514/6.2012-5502.
- [4] Lin YH, Balakrishnan H. Prediction of terminal-area weather penetration on the basis of operational factors. *Transportation Research Board*. 2014;2400(1): 45-53. doi: 10.3141/2400-06.
- [5] Li J, et al. Convective weather avoidance prediction in en route airspace based on support vector machine. *Transactions of Nanjing University of Aeronautics and Astronautics*. 2021;38(4): 656-670. doi: 10.3390/aero-space9040189.
- [6] Sridhar B, Chatterji, G, Grabbe, S, Sheth, K. Integration of traffic flow management decisions. *AIAA*. 2013. doi: 10.2514/6.2002-5014.
- [7] Dwight W, Arthur, W, Heagy, W, Kirk, D. Assessment of prediction error impact on resolutions for aircraft and severe weather avoidance. *AIAA*. 2006. doi: 10.2514/6.2004-6265.
- [8] Isaacson D, et al. Laboratory evaluation of dynamic routing of air traffic in an en route arrival metering environment. *AIAA*. 2018. doi: 10.2514/6.2018-3985.
- [9] Wang L, Wang X, Wei F. Mobile and algorithm of rerouting under adverse weather with moving and shrinking. *Journal of Henan University of Science and Technology (Natural Science)*. 2017;38(03): 35-40. doi: 10.15926/j.cnki.issn1672-6871.2017.03.008.
- [10] Wang F, Wang H. A re-routing path planning method based on Maklink Graph and GA algorithm. *Journal of Transportation Systems Engineering and Information Technology*. 2014;14(5): 154-160. doi: 10.16097/j.cnki.1009-6744.2014.05.058.
- [11] Soler M, Zou B, Hansen M. Flight trajectory design in the presence of contrails: Application of a multiphase mixed-integer optimal control approach. *Transportation Research Part C: Emerging Technologies*. 2014;48: 172-194. doi: 10.1016/j.trc.2014.08.009.
- [12] Zhang Z, Wei Z. A dynamic deviation method for terminal control areas under scattered hazardous weather. *China Safety Science Journal*. 2016;26(1): 40-44. doi: 10.16265/j.cnki.issn1003-3033.2016.01.007.
- [13] Taylor C, et al. Generating diverse reroutes for tactical constraint avoidance. *Air Traffic Control Quarterly*. 2018;26(2): 49-59. doi: 10.2514/1.D0089.
- [14] Taylor C, Wanke C. Improved dynamic generation of operationally acceptable reroutes using network optimisation. *Journal of Guidance, Control, and Dynamics*. 2011;34(4): 961-975. doi: 10.2514/1.52957.
- [15] Xie Z, Zhong Z. Aircraft path planning under adverse weather conditions. *Matec Web of Conferences*. 2016;77:15001. doi: 10.1051/mateconf/20167715001.
- [16] Mao L, Peng Y, Jia Z. Tactical rerouting in severe weather. *Journal of East China Jiaotong University*. 2020;37(02): 72-80. doi: 10.16749/j.cnki.jecjtu.2020.02.010.
- [17] Ayo BS. An improved genetic algorithm for flight path re-routes with reduced passenger impact. *Journal of Computer and Communications*. 2017;05(07): 65-76. doi: 10.4236/jcc.2017.57007.
- [18] Cai K, Tang Y, Wei W. An evolutionary multi-objective approach for network-wide conflict-free flight trajectories planning. *IEEE/AIAA Digital Avionics Systems Conference (DASC)*. 2015;1D2-1-1D2-10. doi: 10.1109/DASC.2015.7311345.
- [19] Taylor C, Wanke C. Generating operationally-acceptable reroutes using simulated annealing. *AIAA*. 2010; 9017. doi: 10.2514/6.2010-9017.
- [20] Chaimatanan S, Delahaye D, Mongeau M. A methodology for strategic planning of aircraft trajectories using simulated annealing. *ISIATM, International Conference on Interdisciplinary Science for Air traffic Management*. 2012. doi: hal-00912772.
- [21] Eduardo A, et al. Informed scenario-based RRT\* for aircraft trajectory planning under ensemble forecasting of thunderstorms. *Transportation Research Part C: Emerging Technologies*. 2021;129: 103232. doi: 10.1016/j.trc.2021.103232.
- [22] Liu, Y, Hansen, M. Predicting aircraft trajectories: A deep generative convolutional recurrent neural networks approach. *ArXiv Preprint ArXiv:1812.11670*. 2018. doi: 10.48550/arXiv.1812.11670.
- [23] Ayhan S, Samet H. Aircraft trajectory prediction made easy with predictive analytics. *Association for Computing Machinery*. 2016; 21-30. doi: 10.1145/2939672.2939694.
- [24] Pang Y, Liu Y. Conditional generative adversarial networks (CGAN) for aircraft trajectory prediction considering weather effects. *AIAA*. 2020; 1853. doi: 10.2514/6.2020-1853.
- [25] Ankerst M, et al. OPTICS: Ordering points to identify the clustering structure. *Association for Computing Machinery*. 1999;28(2): 49-60. doi: 10.1145/304181.304187.
- [26] Krozel J, et al. Capacity estimation for airspaces with convective weather constraints. *AIAA*. 2007; 6451. doi: 10.2514/6.2007-6451.
- [27] Rubnich M, Delaura R. An algorithm to identify robust convective weather avoidance polygons in en route airspace. *AIAA*. 2010; 9164. doi: 10.2514/6.2010-9164.
- [28] Matthews M, Delaura R, Venuti J. Strategic forecasts of TRACON airspace capacity during convective weather impacts. *AIAA*. 2017; 3430. doi: 10.2514/6.2017-3430.